Check for updates

β-cyclodextrin dendritic derivatives as permeation mediators to enhance the *in vitro* albendazole cysticidal activity by the improvement of the diffusion component†

Luis José López-Méndez, [ID] [a] Francisca Palomares-Alonso,[b] Iliana González-Hernández,[b] Helgi Jung-Cook,[bc] Neyra Citlali Cabrera-Quiñones[d] and Patricia Guadarrama*[d]

The improvement of permeation of drugs across parasites' membranes to promote their diffusion component represents a challenge to achieve better therapeutic effects, including the avoidance of drug resistance. In the context of medicinal chemistry, suitable structural modifications can be made, either on a drug or a nanocarrier, to trigger different mechanisms that promote the influx across membranes. This study aimed to demonstrate the potential of a set of dendritic derivatives of β-cyclodextrin (**m2G**, **h2G**, and **m3G**) as nanocarriers, based on their physicochemical and biological behavior in terms of (i) stability, monitored by ^{1}H NMR at pH 7 for seven days, (ii) ability to complex, and subsequently release around 50–80% of the cargo molecule (albendazole) in a biphasic medium and (iii) the absence of *in vitro* cysticidal effect in cysticercus cultures. The albendazole/nanocarrier inclusion complexes (ICs) were proved in the *T. crassiceps* model. According to the EC_{50} values related to the cysticidal activity of albendazole, either free or complexed, the potency of this drug in the ICs experienced a significant increase, which may be attributed to the enhancement of its solubility but also to a better permeation mediated by the amphiphilic dendritic moieties, which ultimately positively impacts the diffusion of this drug through the tegument of the cysticerci. Additional considerations akin to synthetic ease of the dendritic nanocarriers, and production cost, along with the obtained outcomes, allowed us to place **m2G** followed by **m3G** as the best options to be considered for further *in vivo* assays.

Introduction

The development of nanocarriers in the context of macromolecular therapy (MT) is one of the most active areas of medicinal chemistry. This approach has several advantages, either therapeutic, pharmacokinetic, or pharmaceutical, compared to conventional therapies with "naked" drugs.[1,2] Physicochemical properties of hydrophobic bioactive molecules, such as diffusion and aqueous solubility, are upgraded by their nanocarrier-mediated transport through the formation of inclusion complexes (ICs). Consequently, their biopharmaceutical properties above-mentioned[3] are also improved, allowing development of more effective therapies.

For drugs like Albendazole (ABZ), nanocarrier-mediated administration is widely justified since its poor solubility restricts the formulation options.[4] ABZ is a broad-spectrum anthelminthic extensively used,[5] despite its low aqueous solubility. Due to its physicochemical features, ABZ belongs to class II from biopharmaceutical classification system (BCS).[6] This drug requires higher solubility in biological fluids to be absorbed into biological membranes. ABZ frequently fails in treatments of systemic infections such as neurocysticercosis,[7] due to its erratic absorption in the gastrointestinal tract.

Diverse molecular nanoplatforms have been proposed to improve the aqueous solubility and bioavailability of ABZ.[8–11] Nevertheless, it remains a challenge for materials science since its performance to cross biological membranes has not reached a desirable status.

Combining molecular platforms appears as an interesting strategy to form unconventional nanocarriers with the potential to improve the biopharmaceutical properties of drugs such as ABZ. The resulting materials should meet some requisites like

*a*Universidad Autónoma Metropolitana Unidad Xochimilco, Calzada del Hueso 1100, Villa Quietud, Coyoacán, 04960, CDMX, Mexico

*b*Laboratorio de Neuropsicofarmacología, Instituto Nacional de Neurología y Neurocirugía, 14269, CDMX, Mexico

*c*Facultad de Química, Departamento de Farmacia, Universidad Nacional Autónoma de México, 04510, CDMX, Mexico

*d*Instituto de Investigaciones en Materiales, Universidad Nacional Autónoma de México, 04510, CDMX, Mexico. E-mail: patriciagua@materiales.unam.mx
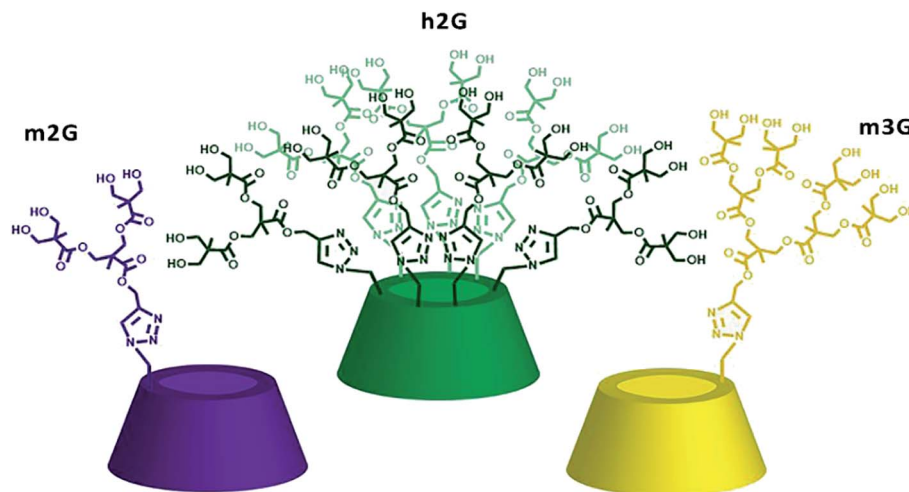
Fig. 1   Three nanocarriers based on the primary face substitution of βCD with polyester dendrons. Mono-substitution-second generation dendron (**m2G**), hepta-substitution-second generation dendron (**h2G**), mono-substitution-third generation dendron (**m3G**).

high-water solubility, low cytotoxicity, stability under physiological conditions, high loading capacity, ease to obtain, and low cost.

Two attractive molecular platforms broadly used in the pharmaceutical industry are cyclodextrins (CDs) and dendrimers. CDs are cone-shaped truncated macrocycles, well-known for hosting hydrophobic molecules within their non-polar cavities forming ICs.

Their potential has been widely utilized in the pharmaceutical industry.[12–14] Among CDs, βCD with seven glucose units is the most used for its size versatility, innocuity, and low cost.[15] Dendrimers, otherwise, are monodisperse structures that have climbed positions towards advanced clinical phases.[16]

Their "lego-like" construction allows multiple derivatizations, including targeting.[17,18] Particularly, polyester-type dendrimers obtained from bis-MPA (2,2-bis(hydroxymethyl) propionic acid) monomer[19] have attracted attention for their high-water solubility, biodegradability, biocompatibility, non-toxicity, and low cost of production.[20] We recently reported the combination of these two molecular platforms by synthesizing a set of nanocarriers based on polyester dendritic derivatives of βCD.[21] Their performance, in terms of drug loading and solubility improvement, was a function of the degree of βCD substitution on its primary face (mono- or hepta-) and the dendron generation (from first to the third generation), taking ABZ as a drug model. The mono-substituted derivatives of the second and third generation, along with the second generation hepta-substituted derivative, shown in Fig. 1 as **m2G**, **h2G**, and **m3G**, exhibited the best compromise between performance and cost, with similar drug loading, around ten times higher, compared with commercial cyclodextrins.[22–24] Given the potential of the above-mentioned molecular systems, the purpose of this study was to evaluate relevant physicochemical and *in vitro* biological aspects to demonstrate their feasibility as nanocarriers and be able to establish the basis to select the most useable one to improve the biopharmaceutical properties of ABZ.

The physicochemical evaluation comprised, in the first place, the stability of **m2G**, **m3G**, and **h2G** at physiological pH (7.4) for seven days, using ¹H NMR as a monitoring tool. Similar degradation times have been reported as meaningful for related carrier systems based on bis-MPA dendrons.[25] ABZ/nanocarrier interactions were investigated by NMR, following the ¹H ABZ signals in ICs formed *in situ*. The physicochemical information concerning the release behavior of the nanocarriers was appraised by the construction of time-dependent ABZ release profiles, using the data from extraction experiments in a biphasic medium (octanol–water).

Regarding the biological performance of the nanocarriers, we conducted *in vitro* assays aimed to study their capability to interact with cellular membranes and promote the diffusion of ABZ as drug model. The permeation of the nanocarriers was correlated to the diffusion of ABZ from the ICs in the vesicular fluid of *T. crassiceps* cysts. The generated outcomes from both physicochemical and biological assays allowed us to demonstrate the role of the dendritic moieties in the improvement of the performance of drugs such as ABZ.

Results and discussion

Degradability under physiological conditions

The compromise between the stability and degradability of nanocarriers at physiologically relevant pH values (*e.g.*, extracellular pH 7.4) is an important matter that impacts their biomedical performance. While their degradation may be related to the loss of targeting functionalities, it also promotes the delivery of the encapsulated drug. Usually, a slow degradation, along with a rapid elimination, are considered limitations of the nanocarriers. When degradation occurs, is also significant the identification of labile sites, where this process may initiate, to be able to correlate the resultant molecular fragments with eventual cytotoxicity. We evaluated the stability of **m2G**, **m3G**, and **h2G** in phosphate-buffered saline (PBS)
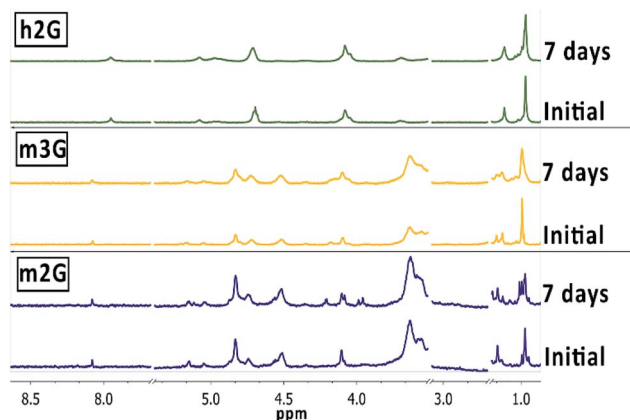
Fig. 2 Stability study at physiological conditions. ^{1}H NMR spectra of m2G, m3G and h2G in DMSO-d$_6$. Comparison between the initial and final time (7 days).

Fig. 3 ^{1}H NMR spectra in DMSO-d$_6$: D$_2$O (3 : 1) of ABZ in ICs with m2G (ABZ-m2G), m3G (ABZ-m3G) and h2G (ABZ-h2G).

solutions (pH 7.4) during seven days at room temperature, recording ^{1}H NMR spectra in DMSO-d$_6$ (Fig. 2).

Under the experimental conditions, nanocarrier m2G exhibited the most noticeable changes in the ^{1}H NMR spectra at around 1.0 ppm, corresponding to the dendritic methyl groups signal, suggesting that the degradation process may begin with the hydrolysis of the peripheral ester bonds at this pH value. The new chemical environment also affected the signals at around 4 ppm, corresponding to the dendritic methylene groups. Previous reports based on MALDI-TOF MS studies demonstrated that the initial step of degradation of polyester dendrimers is the cleavage of the ester bonds, with the loss of fragments corresponding to the benign bis-MPA scaffold.[25] Even though only slight broadenings were observed in the NMR signals of m3G and, to a lesser extent, in the case of h2G, they occurred in the same chemical shift regions, thus confirming the ester bonds as the most probable cleavage sites of the structures. The higher degradability of m2G may be related to the fewer number of ester bonds to be cleaved, compared with the other containers with different numbers of ester bonds, proportionally higher.

Study of inclusion complexes (ICs) by ^{1}H NMR

The ^{1}H NMR spectra of the ICs were acquired in solution, in a mixture DMSO-d$_6$: D$_2$O (3 : 1) as an optimal medium to promote complexation. We studied the interactions in ICs by following the signals of ABZ, bearing in mind the spectrum of free ABZ as a reference, included at the bottom of Fig. 3.

The chemical shifting of the ABZ signals, as the first evidence of the ABZ inclusion, were registered as $\Delta\delta$ (ppm) as shown in Table 1.

The magnitude of the calculated $\Delta\delta$ (ppm) resembled the values reported for this type of ICs.[26] By analyzing the magnitude of this parameter, particularly for the aromatic protons of ABZ, there are notorious differences that allowed us to characterize the nanocarriers in terms of their performance interacting with this drug. As the $\Delta\delta_{ABZ}$-m3G values for protons d, e, and f are the highest, m3G must complex ABZ more efficiently, in
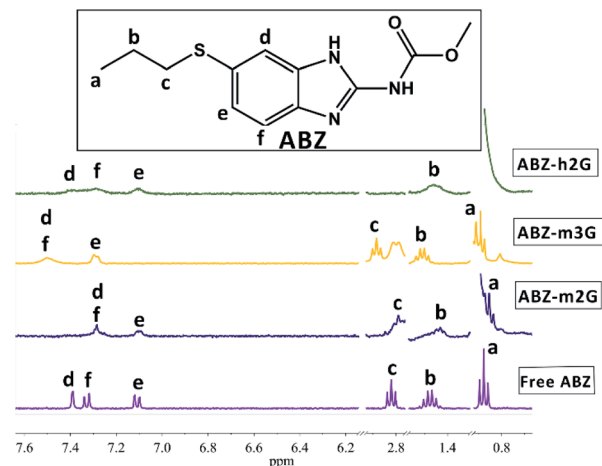
Table 1 ^{1}H Chemical shifts (δ, ppm) corresponding to protons of free ABZ, and complexation induced shifts in the complexed state ($\Delta\delta = \delta_{complex} - \delta_{free}$) in presence of an excess of nanocarrier in DMSO-d$_6$: D$_2$O (3 : 1)

ABZ ^{1}H	Free ABZ δ	ABZ-m2G $\Delta\delta$	ABZ-m3G $\Delta\delta$	ABZ-h2G $\Delta\delta$
H-a	0.88	0.03	0.01	0.04
H-b	1.48	−0.04	0.03	−0.02
H-c	2.82	−0.03	0.07	—
H-d	7.39	−0.1	0.11	0.03
H-e	7.11	−0.01	0.18	−0.01
H-f	7.33	−0.04	0.17	−0.03

comparison with the other two nanocarriers. Moreover, the sign interpretation of $\Delta\delta$ establishes that a negative value accounts for a shielding effect by electronic currents, resulting in upfield shifts, while positive values correspond to a deshielding scenario that shifts the signals downfield. In this sense, the protons of ABZ in ABZ-m3G complex were deshielding, suggesting predominant participation of the third generation dendrons present in this nanocarrier, during the complexation process, while in the case of the other two nanocarriers, though slight, the shielding of the protons point to more assistance of the βCD cavity to form the ICs.

Bearing in mind the structural variables imposed on nanocarriers, m2G and h2G sharing the same dendritic generation, exhibited similar complexing behavior, regardless of the different degree of substitution (-mono or -hepta). Presumably, the flexibility and the number of interaction sites (e.g., to form hydrogen bonds) of the second generation dendrons are not sufficient to contact with the ABZ molecule, and therefore the participation of βCD is promoted. In the case of m3G, the third-generation dendron seems to have a suitable number interacting groups and the flexibility to "surround" the ABZ molecule in a more efficient manner. This information is relevant in terms of nanocarriers design.

Evaluation of nanocarriers release behavior by extractions

To determine the suitability of the nanocarrier systems is necessary to prove the occurrence of the eventual release of the transported drug. Even though dialysis is the most popular and common technique to determine *in vitro* release profiles, the diffusion of the drug molecules from the carrier to the dialysis bags has been recognized as a problem for some carrier systems, delaying the drug appearance in the sampling compartment.[27,28]

To model release profiles of ABZ, we adapted an extraction system on a biphasic medium (octanol–water), usually applied to obtain partition coefficients,[29] incorporating the transference time of the drug between the aqueous and the organic phase as a variable.

The addition of time as a variable during the experiments allowed us to consider dynamics (dissociation-association) involved in these types of supramolecular structures.

As shown in Fig. 4, the total percentage of ABZ extracted from the ICs towards the organic phase varies over time, following different profiles depending on the nanocarrier.

In all the cases occurred the release of ABZ towards the organic phase, evidencing the functional response of **m2G**, **m3G** and **h2G** as nanocarriers to deliver the drug in a medium emulating the hydrophobicity of cell membranes.

The release profiles for all the ICs after 1 hour allowed us to establish the following order in terms of ABZ release percentage: ABZ-**m3G** (79.8%) > ABZ-**m2G** (68.7%) > ABZ-**h2G** (50.1%).

This result is in line with the observations by ^{1}H NMR revealing specific interactions between ABZ and each nanocarrier. As expected, the particular interactions present in each system promoted a differentiated migration toward the organic phase.[30] The mono-substituted nanocarriers **m2G** and **m3G** represent a suitable compromise between synthetic effort and release profiles in a time range typical for oral administration (depending on the drug, from 20 minutes to over an hour).

The highest release percentage of **m3G** might be promoted by the competition of interactions of the third-generation dendron, starting with ABZ, as was circumscribed by NMR, to end with the solvent molecules after solvation in the organic phase.
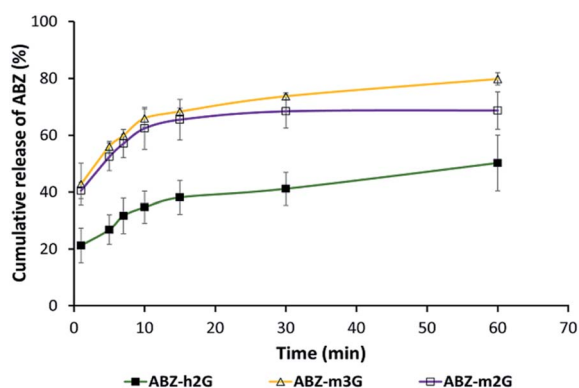
The nanocarrier **h2G** exhibited the highest retention of ABZ in the organic phase, supporting the observations by NMR about the predominant role of the βCD cavity, not of the dendrons, complexing this drug and isolating it from the medium.

Effect of the nanocarriers to promote the diffusion of ABZ to vesicular fluid

In drug delivery processes, a limiting factor for therapeutic efficacy is the lipid-bilayer permeation ability of bioactive molecules that, according to experimental and theoretical studies[29,31] is more complex than a simple diffusion system.[33] The dendritic architecture has demonstrated its suitability to enhance the permeation of co-administered drugs,[31] bearing in mind that the incorporation of appropriate functional groups significantly improves this property[32] by the encouragement of amphiphilic-type interactions.

Taking advantage of the presence of the amphiphilic dendritic moieties on the nanocarriers, we evaluated the assisted diffusion of ABZ contained in ICs (ABZ-**m2G**, ABZ-**m3G** and ABZ-**h2G**) across the tegument of *T. crassiceps* cysticerci, consisting of outer tegument and inner basement membrane.[33]

From different incubation times were calculated the percentages of ABZ in vesicular fluid, related to ABZ in the culture medium (Fig. 5).

Even though either free ABZ, or ABZ from the ICs exhibited a rapid diffusion toward vesicular fluid (more than 20% after 15 minutes), as the experiment proceeded, the percentage of diffused ABZ from the ICs was significantly higher ($p < 0.05$). This tendency was maintained up to 8 hours of incubation, resulting in the following percentages of ABZ found in vesicular fluid: free ABZ (24.65%), ABZ-**m2G** (45.26%), ABZ-**m3G** (42.00%), and ABZ-**h2G** (49.23%). It can be seen that the percentage of ABZ in ABZ-**h2G** was slightly higher in
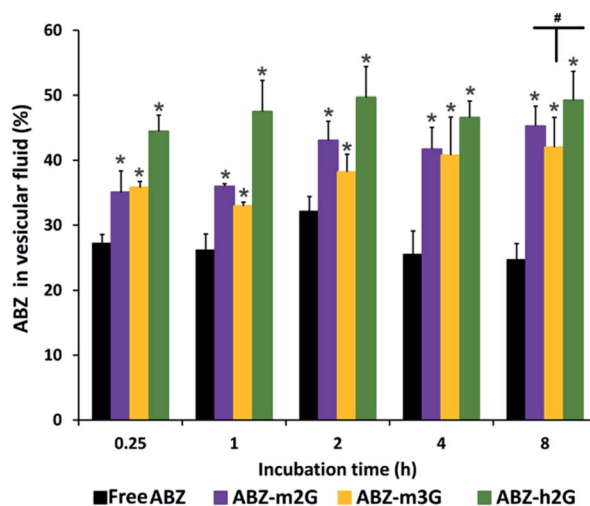
Fig. 4 Release profiles by extraction experiments over time of ABZ on a biphasic medium (octanol–water). Each point represents the mean of percentage of ABZ found in the organic phase ±SD $n = 3$.

Fig. 5 ABZ diffusion to vesicular fluid of *Taenia crassiceps* cysts (percentage of ABZ found in vesicular fluid ±SD) after *in vitro* exposure to: free ABZ (black bars) and ABZ-ICs (purple, yellow and green bars). $n = 3$. *$p < 0.05$ against free ABZ. #$p > 0.05$ between dendritic nanocarriers.

comparison with the other nanocarriers, however no statistical differences between the ICs were found ($p > 0.05$).

The enhanced diffusion of ABZ, mediated by the dendritic nanocarriers, may be discussed in terms of the macromolecular therapy concepts. Beyond the evident impact of high molecular weights onto permeation, the covalent construction of **m2G**, **m3G**, and **h2G** guarantees a defined distribution of the neutral hydroxyl groups at the surface that may be benefiting their permeation by precise and collective interactions with biological counterparts, like membranes.[34–37]

The amphiphilicity of dendritic nanocarriers represents a further contribution to the nanocarriers behavior. Considering that biological membranes are composed of amphiphilic molecules (phospholipids/cholesterol in aqueous media), the hydrophobic/hydrophilic balance of **m2G**, **m3G**, and **h2G** seems to favor their permanence in the environment of the bilayer, either onto the surface or penetrating the cellular membrane.

The transport of ABZ, assisted by the nanocarriers, resulted in a more successful diffusion of this drug.

In vitro cysticidal activity

To assert or discard a possible cysticidal activity of the nanocarriers was carried out their evaluation in the assay conditions, in the absence of ABZ. Following the procedure described to evaluate the cysticidal activity, were obtained images by inverted light microscope (ILM), as shown in Fig. 6. After 11 days of treatment, the cysts (*T. crassiceps* metacestodes) incubated either in culture medium (Fig. 6A) or in the presence of dendritic nanocarriers (Fig. 6B), showed that they were alive, exhibiting normal morphology, size, and motility in terms of alternating movements of contraction and relaxation. The observations here presented for the parasites treated with **m2G** were replicated for the other dendritic nanocarriers (see Fig. S4†). These results corroborated that nanocarriers had no cysticidal activity over the cysts. Parasites treated with ABZ, either free or from the corresponding IC, displayed concentration-dependent morphological changes such as a gradual loss of the vesicular fluid, size reduction, and shape change (Fig. 6C). These observations are in agreement with the previously reported activity of this drug.[38]

To quantify the cysticidal effect of ABZ were constructed concentration–response curves for this drug, both free and contented in the ICs (Fig. 7). In all the cases the activity was concentration-dependent.

Fig. 7 Cysticidal activity. Concentration-response curves of free ABZ and ABZ in ICs. Each point represents the mean ± SE. $n = 6$.

The EC_{50} values, either for free or complexed ABZ, were determined and shown in Table 2. These values, related to the drug concentrations required for 50% mortality, demonstrated that the assistance of the dendritic nanocarriers transporting ABZ potentiated its intrinsic activity nearly double.

It is well-known that the poor ABZ aqueous solubility restricts its efficacy. As the diffusive contribution depends on the drug solubility,[39,40] the enhancement of the ABZ solubility, in the presence of the dendritic nanocarriers, improved its diffusion through the tegument of the cysts, thus impacting its

Table 2 Comparison of EC_{50} values from the *in vitro* assay

ABZ system	EC_{50} values (μM)
Free	0.45 (0.36–0.63)[a]
ABZ-**m2G**	0.26 (0.16–0.33)[a]
ABZ-**m3G**	0.28 (0.15–0.36)[a]
ABZ-**h2G**	0.25 (0.20–0.31)[a]

[a] Confidence interval at 95%.

Fig. 8 Indirect carrier structure-ABZ activity relationship. Correlation at 8 h between diffusion and cysticidal activity of ABZ.
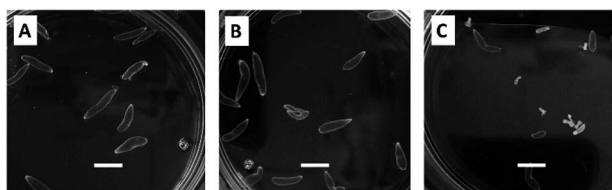

Fig. 6 Morphological appearance of *T. crassiceps* cysts after *in vitro* treatments. (A) control group (0.19% DMSO in DMEM), (B) **m2G** dendritic nanocarrier (7.24 μM) and (C) ABZ (0.45 μM). Bars represent 3 mm.
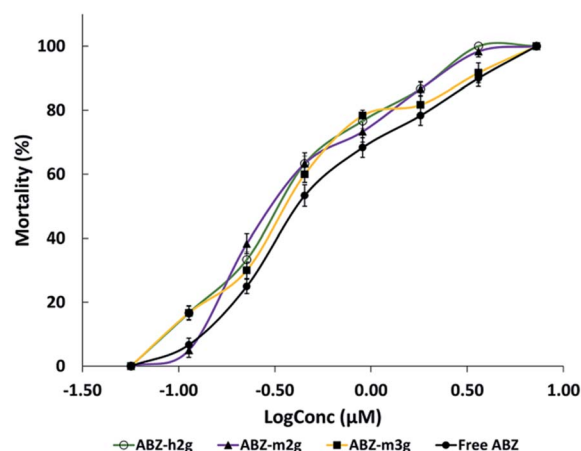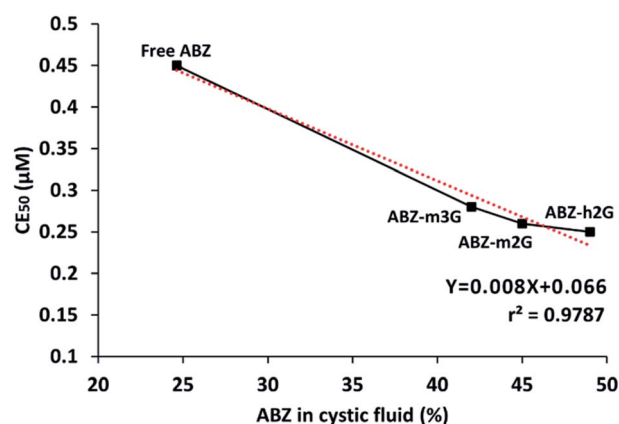
Table 3 Qualitative ranking of **m2G**, **m3G** y **h2G**

Nanocarrier	Synthetic ease	Low-cost production	Degradability	Release of ABZ	Total Score
m2G	3	3	3	2	11
m3G	2	2	2	3	9
h2G	1	1	1	1	4

potency positively. Similar outcomes for ABZ have been reported to improve its solubility-efficacy duo, using different molecular platforms.

The biological response of ABZ in the ICs is also attributable to the permeation increase, as discussed before, which promotes its diffusion more efficiently. Analyzing the dendritic structural parameters of each nanocarrier, all of them are different. With βCD as a constant, each container differs on the number of hydroxyl peripheral groups, and the sterical hindrance imposed by different size generations or degree of substitution on βCD. Despite these differences, a high correlation ($R = 0.9787$) was observed by plotting the free or complexed ABZ cysticidal efficacy based on EC_{50} values *versus* the percentage of this drug found in the vesicular fluid (Fig. 8).

The fact that the three ICs are in a common region on the graph allow us to presume that the sum of the structural effects in each case results in a comparable impact on the cysticidal activity of ABZ. The observed correlation hence may be described as an indirect carrier structure-ABZ activity relationship.

Even though the biological performance of free ABZ was significantly different from ABZ carried in the ICs, the small differences observed for complexed ABZ in the ICs did not allow choosing the best option with this criterion.

In this context, the selection of the most suitable nanocarrier for further *in vivo* assays might consider other indicators such as the synthetic ease, mainly based on the reaction time, low-cost of production, in terms of quantities of the raw materials, degradability at physiological conditions, and release ability of ABZ. A qualitative ranking of the nanocarriers considering these indicators is provided in Table 3, where a numerical scale (from 1 to 3) were established, where 1 and 3 are the worst and the best qualifications respectively.

Under these considerations, **m2G** gathers the most favorable qualification, but the overall performance of **m3G** also makes it a suitable candidate. Therefore, these two platforms may be the most appropriate for subsequent biological evaluations as ABZ carriers.

Table 4 Optimized MS/MS parameters for ABZ and IS

Analyte	MRM transition m/z	DP^a (V)	EP^b (V)	CE^c (V)	CXP^d (V)
ABZ	266.3 → 234.0	34	4.5	25	3.0
IS	237.2 → 194.1	43	4.0	22	3.0

[a] DP: declustering potential. [b] EP: entrance potential. [c] CE: collision energy. [d] CXP: collision exit potential.

Conclusions

From materials science, and in the context of medicinal chemistry, were proposed the molecular platforms **m2G**, **m3G**, and **h2G** as nanocarriers to improve the biopharmaceutical properties of highly hydrophobic drugs such as ABZ.

Respectively, the experiments of NMR and ILM demonstrated relevant characteristics of the nanocarriers like their degradability under physiological conditions, and their harmless toward the biological model of *T. crassiceps* cysts.

The NMR tracking of interactions between ABZ and nanocarriers allowed us to suggest different host–guest interactions, depending on the nanocarrier. These observations were in line with the results obtained from the modeled-release experiment, where was evident a differentiated migration toward the organic phase.

The enhanced diffusion of the complexed ABZ crossing the tegument of *T. crassiceps* cysticerci evidenced the role of the amphiphilic dendrons to mediate the drug passage through cellular membranes. Furthermore, we observed a high correlation between the ABZ diffusion and its cysticidal activity, which is indirectly related to a better permeation promoted by the dendritic nanocarriers.

The EC_{50} values allowed us to conclude that the potency of free ABZ was the lowest throughout the entire concentration range under study. The ABZ solubility enhancement, along with the improved permeation mediated by the dendritic nanocarriers, resulted in an increase in the cysticidal effect of the complexed ABZ.

Even though *in vivo* assays are required to confirm the efficacy and safety of the dendritic nanocarriers, the *in vitro* results place these materials as very promising molecular containers to improve the solubility, permeation, and, consequently, the potency of ABZ or potentially of any other hydrophobic drug.

Experimental

Materials and reagents ABZ (≥98%), methanol (≥98%), octanol (anhydrous, ≥99%), sodium phosphate dibasic heptahydrate (≥98%), and potassium phosphate monobasic (≥99%) were analytical grade, acquired from Sigma-Aldrich Chemical Co. (St. Louis, MO, USA) and used as received. Deuterated dimethylsulfoxide (DMSO-d_6, deuteration degree 99.5%) and deuterium oxide (D$_2$O, deuteration degree 99.9%) were acquired from Cambridge Isotope Laboratories, Inc. (Andover. USA). Ultrapure water was purified by a Millipore Milli Q Water Purification System (Millipore, Bedford, MA, USA). Nanocarriers **m2G**, **m3G**, and **h2G** (Fig. 1) were synthetized according to previously reported procedures.[21]

For *in vitro* assays was used Dulbecco's modified Eagle's medium–high glucose (DMEM) from Sigma-Aldrich Chemical Co (St. Louis, MO, USA). DMEM was supplemented with 10% fetal calf serum, 2 mM L-glutamine, 8 mg dL^{-1} of gentamicin sulfate and 200 000 IU dL^{-1} of penicillin G sodium (Gibco, Milpitas, CA, USA). Dimethyl sulfoxide (DMSO; J.T. Baker, Mexico, México; assay 99%) was analytical reagent grade.

Taenia crassiceps cysts T. crassiceps cysticerci (ORF strain) were obtained from female BALB/c mice, experimentally infected according to a procedure previously described.[41] Briefly, mice were killed by cervical dislocation and the cysts were extracted from the peritoneal cavity and washed three times with 0.9% sterile saline solution. For the experiments were selected cysts from 2–3 mm, no budding, with a translucent membrane and exhibiting intact bladder surface. The protocol was approved by the Institutional Committee for Handling and Animal Care of Instituto Nacional de Neurología y Neurocirugía (registration number 51/15) and was conducted under the Mexican Official Regulations (NOM-062-ZOO-1999).

Equipment NMR spectra were recorded on Bruker Avance spectrometer (400 MHz for ^{1}H and 100 MHz for ^{13}C) at 25 °C. UV-vis spectra were recorded on a spectrophotometer model UV300 UNICAM with a quartz cell of 1 cm path length. All measurements were carried out at room temperature.

The concentration of ABZ in the vesicular fluid was determined using LC-MS/MS. The system consisted of an Agilent 1100 HPLC (quaternary pump and autosampler) (Palo Alto, CA, USA) coupled to an ABSciex 3200 QTrap linear ion trap quadrupole mass spectrometer (ABSciex, Darmstadt, Germany) with an electrospray ionization (ESI) interface, which was operated in the positive ionization mode. Data acquisition and processing were performed using the Analyst software 1.6.2 version (Applied Biosystems, Foster City, CA, USA), and quantitative analysis was performed using MultiQuant software version 3.0 (Applied Biosystems, Foster City, CA, USA).

Methods

Evaluation of the degradability of nanocarriers **m2G**, **m3G** and **h2G** by ^{1}H NMR. The stability of nanocarriers was evaluated at physiological pH for seven days. Each nanocarrier (10 mg) was dissolved in 10 mL of phosphate-buffered saline (PBS) solution and kept at 37 °C during the entire experiment. 1 mL aliquots of each solution were collected at specific times for seven days and stored at −8 °C until they were used. To carry out the ^{1}H NMR experiment of each sample, the corresponding nanocarrier aliquot at a specific time, was lyophilized and re-dissolved in 0.5 mL of DMSO-d$_6$ to be analyzed.

Preparation of inclusion complexes (ABZ/nanocarrier) and quantification of ABZ. In a round-bottom flask was dissolved the corresponding nanocarrier (0.045 mmol) in 3 mL of water and were added 0.090 mmol of ABZ to the solution. The resulting suspensions were vigorously stirred at 50 °C for 5 days, and subsequently filtered and lyophilized to obtain the corresponding IC. To quantify the complexed ABZ was prepared a calibration curve from a 7.54 mM stock solution of ABZ in methanol, diluting to obtain 8 points with concentrations in the range 0.02–0.11 mM. These solutions were analyzed by UV-vis at 298 nm. Subsequently, 5.0 mg of each IC were diluted in methanol, in a 5 mL volumetric flask. The resulting solutions were analyzed by UV-vis, and the obtained absorbances were interpolated into the calibration curve (Fig. S1†). The experiment was performed in triplicate for each IC. The amount of ABZ found on each IC was expressed as mg of ABZ per mmol of nanocarrier.

^{1}H NMR study of the ICs formed *in situ*. The NMR technique, extensively used for studying ICs,[43] was chosen to identify interaction sites between nanocarriers and ABZ. ^{1}H NMR experiments were conducted at room temperature. First, a solvent mixture DMSO-d$_6$:D$_2$O in a ratio of 3 : 1 was prepared and used for the preparation of ABZ and each nanocarrier solutions. The spectrum of free ABZ was acquired from a 2 mM solution, taking 0.5 mL as the initial volume. Thereafter, the addition of a 40 mM solution (0.150 mL) of the corresponding nanocarrier, under vigorous stirring for 1 minute, allowed us the *in situ* formation of ICs, and their posterior analysis by ^{1}H NMR.

Extraction profiles of ABZ by organic/aqueous phase transfer

To model the ABZ release from the ICs, an organic/aqueous transfer medium was prepared in the first place, mixing equivalent volumes of octanol and ultrapure water and allowing the saturation between phases. After the equilibrium was attained, the phases were separated and used for the experiments. The organic phase previously saturated (3 mL) was added to aqueous solutions of each IC containing 0.06 mM of ABZ and the mixtures were vigorously stirred at room temperature for 1 minute. Afterward, the system was allowed to equilibrate for 5 minutes to achieve the complete separation of phases. An aliquot of 0.5 mL was taken from the organic phase and analyzed by UV-vis, with reposition of the original solution with 0.5 mL of the saturated organic phase. From the solutions under stirring were taken consecutive aliquots at 5, 7, 15, 30, and 60 minutes, following the same procedure. The concentration of extracted ABZ from ICs was determined by interpolation on a calibration curve previously prepared from a 7.54 mM stock solution of ABZ in octanol, with eight points at a concentration range from 0.02 to 0.10 mM, taking the absorption maximum at 298 nm for each point (Fig. S3†).

The percentage of ABZ found in the organic phase was calculated with eqn (1).

$$\%\text{ABZ in the organic phase} = C_{ABZo}*100/C_{ABZi} \quad (1)$$

where C_{ABZo} is the concentration in the organic phase, and C_{ABZi} is the initial concentration of ABZ, in this case 0.06 mM for all the ICs.

A cumulative percentage of released ABZ in the organic phase was obtained and plotted *versus* time. The assays were performed in triplicate.

In vitro assay on *T. crassiceps cysticerci*. The nanocarriers' ability to assist the permeation in the cysticerci was indirectly evaluated by the quantification of ABZ diffused from the ICs to vesicular fluid. To ensure a reliable quantification of ABZ, we used an initial concentration higher than the IC$_{50}$ value (0.45

μM). A stock solution of ABZ (3.8 mM in DMSO) was serially diluted in distilled water to obtain a working solution of ABZ 3.8 μM in DMEM. The same serial dilutions were performed for ICs in water to achieve an equivalent net concentration of ABZ of 3.8 μM. Cell-culture flasks were carefully filled with 5 mL of either ABZ or ICs solutions. Then, 50 cysts were deposited into each flask and incubated at 37 °C in a 5% CO_2 atmosphere, and 98% of relative humidity. The cysts were incubated at 0.25, 1, 2, 4, and 8 h, each one by triplicate.

After incubation, the cysts were washed three times with sterile 0.9% saline solution, placed in Petri dishes and ruptured individually using a needle. The released vesicular fluid from each dish was collected using a Pasteur pipette and transferred to centrifuge tubes to be centrifuged at 3000 rpm for 10 minutes. The supernatant culture medium and the vesicular fluid were stored at −70 °C until analyzed.

Quantification of ABZ in vesicular fluid and culture medium. To quantify the ABZ able to diffuse into the cellular environment, the samples of the *in vitro* assay on *T. crassiceps cysticerci* were analyzed by LC-MS/MS spectrometry.

Aliquots of 100 μL either from the vesicular fluid or culture medium, were transferred to assay tubes and spiked with 100 μL of carbamazepine (internal standard, IS, 0.2 mg mL^{-1}). ABZ was extracted using 5 mL of a mixture of ether:dichloromethane:chloroform (60 : 30 : 10, v/v/v) with vortex-shaking for 5 minutes. Then, samples were centrifuged at 3000 rpm for 20 minutes, and frozen at −70 °C for 20 minutes. The organic supernatants were transferred to clean tubes and evaporated to dryness at 60 °C under a nitrogen stream. The dried extracts were reconstituted with 50 μL of mobile phase and a volume of 10 μL was injected into the chromatographic system. The detection limit of the method was 2.5×10^{-2} μg mL^{-1} ABZ, and the assay range was $2.5–8.0 \times 10^{-2}$ μg mL^{-1}.

The chromatographic separation was performed on a Gemini C_{18} analytical column (150 × 4.6 mm, 5 μm, Phenomenex, Torrance, CA, USA) attached to a pre-column (Phenomenex C_{18} ODS). A mixture of methanol and 20 mM formic acid in water (70 : 30 v/v) was used as a mobile phase, applying a flow rate of 0.7 mL min^{-1}. ABZ and the IS, were detected in the positive ionization mode with electrospray ionization (ESI) using the following mass spectrometer settings: curtain gas 20 psi, ion spray voltage 5500 V, capillary temperature 600 °C, nebulization gas 50 psi, heating gas 40 psi. Quantification was performed using multiple reaction monitoring of the following transitions: *m/z*: 266.3 → 234 for ABZ and 237.2 → 194.1 for the IS.

Table 4 shows the optimum MS parameters for ABZ and IS. The percentage of ABZ found in vesicular fluid was calculated using the eqn (2):

$$\text{ABZ in vesicular fluid (\%)} = (\text{CABZb} * 100)/(\text{CABZa}) \quad (2)$$

where CABZa is the ABZ concentration in culture medium, and CABZb is ABZ concentration in vesicular fluid.

Cysticidal activity on *T. crassiceps* Stock solutions of ABZ and ICs were prepared in DMSO and water respectively, with ABZ equivalent concentrations of 3.7 mM (1 mg mL^{-1}). Aliquots of

0.1 mL of the stock solutions were taken and diluted with water to obtain the working solutions of 100 μg mL^{-1} of ABZ or ICs.

Different aliquots of the working solutions were taken to prepare the solutions of ABZ or ICs in DMEM to achieve the following concentrations: 0.06, 0.11, 0.23, 0.45, 0.90, 1.81, 3.62 and 7.24 μM. DMSO 0.19% in DMEM was prepared as negative control. Also, each nanocarrier without ABZ (**m2G**, **m3G**, and **h2G**) was dissolved in water at the maximum concentration used in the study (7.24 μM) to evaluate its effect on the parasite. Twenty-four well cell culture flat-bottom microplates (NUNC, Denmark) were used for the assay. Ten cysts were placed into each well and were filled with a final volume of 2 mL of DMEM containing ABZ, ICs or the control. The microplates were incubated at 37 °C with 5% CO_2 atmosphere and 98% of relative humidity for 11 days. The culture medium was changed every two days. The parasites were observed every day, and the mortality was registered using an inverted light microscope (ILM) ICM 405 (Carl Zeiss Inc., USA). The criteria to assess parasite mortality were loss of vesicular fluid, paralysis of the membrane and collapse of parasites.[42] On day 12, the mortality of parasites was established using the Trypan Blue exclusion test (Louis, K.S., Siegel, A.C., 2011). To evaluate the effect of each treatment *in vitro*, a sample of living cysts was extracted on day 12 and observed under the microscope. Parasite morphological changes, including alterations in shape and size, were identified by ILM after washing them with 0.9% saline solution.

The values of EC$_{50}$ (effective concentration of each compound to kill 50% of the cysts), and 95% confidence limits, were calculated by the concentration–response curves using the Hill's equation and the GraphPad software (Prism, version 8 for Windows, U.S.A.). All treatments were performed in sextuplicate.

Statistical analysis

The results of nanocarriers' permeation on *T. crassiceps cysts*, assessed by the quantification of ABZ in vesicular fluid, were analyzed by ANOVA using the Dunnet's test as a post-test, considering free ABZ as control. A Tukey's test was performed in order to detect differences between nanocarriers permeation. To evaluate the differences between the EC50 values, we performed a *t*-test. In all cases, differences were considered significant at $p < 0.05$. Statistical analysis was carried out using SPSS software (V. 15.0).

Author contributions

L. J. López-Méndez: conceptualization, investigation, methodology, visualization writing – original draft. F. Palomares-Alonso: investigation, methodology, formal análisis, writing – original draft. I. González-Hernández: investigation. H. Jung-Cook, resources supervision. N. C. Cabrera-Quiñones, investigation, methodology, formal analysis. And P. Guadarrama conceptualization, funding acquisition, resources, Supervision, writing – original draft, writing – review and editing.

Conflicts of interest

There are no conflicts to declare.

Acknowledgements

Notes and references

1 J. Hu, Y. Cheng, Y. Ma, Q. Wu and T. Xu, *J. Phys. Chem. B*, 2009, **113**, 64–74.

2 D. Soto-Castro, J. A. Cruz-Morales, M. T. R. Apan and P. Guadarrama, *Bioorg. Chem.*, 2012, **41**, 13–21.

3 Y. Vikas, K. Sandeep, D. Braham, C. Manjusha and V. Budhwar, *Asian J. Pharm.*, 2018, **12**, S394–S409.

4 B. Pradines, J.-F. Gallard, B. I. Iorga, C. Gueutin, P. M. Loiseau, G. Ponchel and K. Bouchemal, *Carbohydr. Res.*, 2014, **398**, 50–55.

5 J. Horton, Albendazole: A review of anthelmintic efficacy and safety in humans, *Parasitol*, 2000, **121**, 113–132.

6 Y. Kawabata, K. Wada, M. Nakatani, S. Yamada and S. Onoue, *Int. J. Pharm.*, 2011, **420**, 1–10.

7 H. Jung-Cook, *Expert Rev. Clin. Pharmacol.*, 2012, **5**, 21–30.

8 P. Panwar, B. Pandey, P. C. Lakhera and K. P. Singh, *Int. J. Nanomed.*, 2010, **5**, 101.

9 A. García, D. Leonardi, M. O. Salazar and M. C. Lamas, *PLoS One*, 2014, **9**, e88234.

10 S. G. Castro, S. F. Sanchez Bruni, L. P. Urbizu, A. Confalonieri, L. Ceballos, C. E. Lanusse, D. A. Allemandi and S. D. Palma, *Pharm. Dev. Technol.*, 2013, **18**, 434–442.

11 M. G. Barrera, D. Leonardi, R. E. Bolmaro, C. G. Echenique, A. C. Olivieri, C. J. Salomon and M. C. Lamas, *Eur. J. Pharm. Biopharm.*, 2010, **75**, 451–454.

12 J. Rincón-López, Y. C. Almanza-Arjona, A. P. Riascos and Y. Rojas-Aguirre, *J. Drug Delivery Sci. Technol.*, 2021, **61**, 02156.

13 T. Loftsson, D. Hreinsdóttir and M. Másson, *Int. J. Pharm.*, 2005, **302**, 18–28.

14 P. Jansook, N. Ogawa and T. Loftsson, *Int. J. Pharm.*, 2018, **535**, 272–284.

15 M. E. Brewster and T. Loftsson, *Adv. Drug Delivery Rev.*, 2007, **59**, 645–666.

16 L. Wu, M. Ficker, J. B. Christensen, P. N. Trohopoulos and S. M. Moghimi, *Bioconjugate Chem.*, 2015, **26**, 1198–1211.

17 C. C. Lee, J. A. MacKay, J. M. J. Fréchet and F. C. Szoka, *Nat. Biotechnol.*, 2005, **23**, 1517–1526.

18 J. Twibanire and T. B. Grindley, *Polymers*, 2014, **6**, 179–213.

19 A. Carlmark, E. Malmström and M. Malkoch, *Chem. Soc. Rev.*, 2013, **42**, 5858.

20 O. L. Padilla De Jesús, H. R. Ihre, L. Gagne, J. M. J. Fréchet and F. C. Szoka, *Bioconjugate Chem.*, 2002, **13**, 453–461.

21 L. J. López-Méndez, E. E. Cuéllar-Ramírez, N. C. Cabrera-Quiñones, Y. Rojas-Aguirre and P. Guadarrama, *Int. J. Biol. Macromol.*, 2020, **164**, 1704–1714.

22 C. Moriwaki, G. L. Costa, C. N. Ferracini, F. F. De Moraes, G. M. Zanin, E. A. G. Pineda and G. Matioli, *Braz. J. Chem. Eng.*, 2008, **25**, 255–267.

23 C. G. de Melo, L. A. G. da Costa, M. M. Rabello, V. de Albuquerque Wanderley Sales, A. S. Ferreira, P. C. D. da Silva, R. H. V. Nishimura, R. M. F. da Silva, L. de Araújo Rolim and P. J. R. Neto, *Curr. Drug Delivery*, 2022, **19**, 86–92.

24 J. Priotti, M. V. Baglioni, A. García, M. J. Rico, D. Leonardi, M. C. Lamas and M. Menacho Márquez, *AAPS PharmSciTech*, 2018, **19**, 3734–3741.

25 N. Kalva, N. Parekh and A. V. Ambade, *Polym. Chem.*, 2015, **6**, 6826–6835.

26 R. Zhao, C. Sandström, H. Zhang and T. Tan, *Molecules*, 2016, **21**, 1–11.

27 M. Yu, W. Yuan, D. Li, A. Schwendeman and S. P. Schwendeman, *J. Controlled Release*, 2017, **520**, 181–194.

28 S. Simovic and C. A. Prestidge, *Eur. J. Pharm. Biopharm.*, 2007, **67**, 39–47.

29 C. D. Schönsee and T. D. Bucheli, *J. Chem. Eng. Data*, 2020, **65**, 1946–1953.

30 E. Kaunisto, M. Marucci, P. Borgquist and A. Axelsson, *Int. J. Pharm.*, 2011, **418**, 54–77.

31 A. V. Thomae, T. Koch, C. Panse, H. Wunderli-Allenspach and S. D. Krämer, *Pharm. Res.*, 2007, **24**, 1457–1472.

32 A. V. Thomae, H. Wunderli-Allenspach and S. D. Krämer, *Biophys. J.*, 2005, **89**, 1802–1811.

33 W. Shinoda, *Biochim. Biophys. Acta, Biomembr.*, 2016, **1858**, 2254–2265.

34 Y. L. Wang, Z. Y. Lu and A. Laaksonen, *Phys. Chem. Chem. Phys.*, 2012, **14**, 8348–8359.

35 M. Voge, *J. Parasitol.*, 1963, **49**, 85.

36 B.-C. Wang and C.-Y. Cheng, *J. Mol. Struct.: THEOCHEM*, 1997, **391**, 179–187.

37 A. Bhardwaj, L. Kumar, S. Mehta and A. Mehta, *Artif. Cells, Nanomed., Biotechnol.*, 2015, **43**, 299–310.

38 S. S. Das, P. Bharadwaj, M. Bilal, M. Barani, A. Rahdar, P. Taboada, S. Bungau and G. Z. Kyzas, *Polymers*, 2020, **12**, 1397.

39 F. Palomares-Alonso, J. C. Piliado, G. Palencia, A. Ortiz-Plata and H. Jung-Cook, *J. Antimicrob. Chemother.*, 2007, **59**, 212–218.

40 M. K. Bommaka, M. C. Mannava, K. Suresh, A. Gunnam and A. Nangia, *Cryst. Growth Des.*, 2018, **18**, 6061–6069.

41 R. Bettini, P. L. Catellani, P. Santi, G. Massimo, N. A. Peppas and P. Colombo, *J. Controlled Release*, 2001, **70**, 383–391.

42 F. Palomares-Alonso, I. S. Rojas-Tomé, V. Juárez Rocha, G. Palencia Hernández, A. González-Maciel, A. Ramos-Morales, R. Santiago-Reyes, I. E. González-Hernández and H. Jung-Cook, *Exp. Parasitol.*, 2015, **156**, 79–86.

43 M. Kfoury, D. Landy and S. Fourmentin, *Molecules*, 2018, **23**, 1204.